Maximum Hands-Off Attitude Control*

Sigrid Kjønnø Schaanning[1], Bjørn Andreas Kristiansen[1], Jan Tommy Gravdahl[1]

***Abstract*— In this paper, we explore the use of maximum hands-off control for attitude control of a spacecraft actuated by reaction wheels. The maximum hands-off, or L_0-optimal, controller aims to find the sparsest control signal among all admissible control signals. L_0-optimal problems are generally hard to solve as L_0-cost functions are discontinuous and non-convex. Previous research have investigated methods to approximate the L_0-norm in the cost function, for instance by using an L_1-norm. We propose an approach to the maximum hands-off control problem for spacecraft attitude control involving an L_0-cost function relaxed through complementarity constraints. The controller is applied to the spacecraft attitude control problem, and the performance of the maximum hands-off controller is compared to that of the L_1-optimal controller. Simulations of a 6U CubeSat were conducted using CasADi as the primary optimization tool, and the L_1- and L_0-optimal control problems were discretized using direct multiple-shooting and solved using the IPOPT solver. In addition to these results, we propose a new control scheme, called *moving* maximum hands-off control, which lets the user specify in which time interval the control should occur, and then aims to find the sparsest control among all admissible controls based on this information. The moving maximum hands-off controller is demonstrated to be as sparse as the maximum hands-off controller for some spacecraft maneuvers.**

I. INTRODUCTION

Attitude control of spacecraft is a field in which multiple studies have been conducted [1]–[3]. Several solutions have been suggested to solve the spacecraft attitude control problem, such as proportional-derivative (PD) control laws [1], [4]. Optimal control has been applied for spacecraft attitude control in multiple cases, and with the use of different cost functions. For instance, a time optimal attitude control problem has been studied, where the objective is to minimize the time it takes to rotate a rigid body to a desired attitude and angular velocities, while subject to control input constraints [5]. A cost function based on angular velocity has been used to optimize the attitude motion planning of a spacecraft, with pointing and actuator constraints [6].

Maximum hands-off control has, to the authors' best knowledge, not been applied to spacecraft attitude control. However, a single-axis version of the problem has been studied in [7]. A maximum hands-off controller is a type of optimal controller with control values which are most often zero, i.e., the control values are *sparse*, but still manage to achieve the control objectives [8]. A hands-off controller holds the control values at exactly zero over a time interval, and the *maximum* hands-off controller maximizes the time interval over which the control input is exactly zero [9]. This is a desirable property in systems where resources are limited such as in spacecraft (attitude) control.

The main contribution of this paper is the design of a maximum hands-off controller solving the attitude control problem for a spacecraft actuated by reaction wheels. The maximum hands-off controller is tested through simulations of a 6U CubeSat which resembles the configuration of HYPSO-1 [10]. HYPSO-1 is a smallsat actuated by reaction wheels and developed at NTNU [10]. We furthermore design and implement the moving maximum hands-off controller as an extension to the maximum hands-off controller. The moving maximum hands-off controller allows the user to specify in which time interval the control inputs should occur and is, to the authors' best knowledge, a novel concept within control. Finally, this paper provides a comparison of the responses of the maximum hands-off controller, the moving maximum hands-off controller, and the L_1-optimal controller when solving the spacecraft attitude control problem.

The rest of this paper is organized as follows: Section II describes the coordinate frames and presents the spacecraft dynamics. Section III introduces theory behind the maximum hands-off controller. Section IV introduces the controller designs, including the design of the novel moving maximum hands-off controller, and Section V presents the simulation setup. The simulation results are presented in Section VI, whereas the findings are discussed in Section VII. Section VIII provides the conclusion.

II. SPACECRAFT MODEL

In this section, we present the model of a spacecraft orbiting the Earth, actuated by reaction wheels.

A. Coordinate frames

A reference frame, or a coordinate frame, is a choice of coordinate system given as $\{r\} = \{O_r, \mathbf{x}_r, \mathbf{y}_r, \mathbf{z}_r\}$, where O_r is the origin and $\mathbf{x}_r, \mathbf{y}_r, \mathbf{z}_r$ are orthonormal unit vectors.

1) Earth-centered inertial (ECI) frame: The ECI frame, denoted $\{i\}$, is considered to be an inertial frame. The origin of $\{i\}$ is located at the Earth's center of mass, with the z-axis pointing through the North Pole, the x-axis pointing towards the vernal equinox and the y-axis completes the right-hand system [11].

2) Body frame: The body frame, denoted $\{b\}$, is a coordinate frame fixed to the spacecraft, with origin at the spacecraft's center of mass [11]. The body frame axes follow the spacecraft structure.

*The work is sponsored by the Research Council of Norway through the Centre of Excellence funding scheme, project number 223254, AMOS.

[1]The authors are with the Department of Engineering Cybernetics at NTNU Norwegian University of Science and Technology, NO-7491 Trondheim, Norway. Bjørn Andreas Kristiansen and Jan Tommy Gravdahl are also affiliated with the NTNU Centre for Autonomous Marine Operations and Systems. E-mails: sigrid.schanning@gmail.com, {bjorn.a.kristiansen, jan.tommy.gravdahl}@ntnu.no

3) Orbit frame: The Local Vertical, Local Horizontal (LVLH) frame, or the orbit frame, is denoted $\{o\}$ and has origin at the spacecraft's center of mass. The z-axis points in the direction of the Earth's center of mass, the x-axis points in the direction of the orbit velocity vector, while the y-axis completes the right-handed coordinate system. The unit vectors of the orbit frame are defined as [12]

$$\hat{\mathbf{z}}^o = -\frac{\mathbf{r}^i}{\|\mathbf{r}^i\|_2},\ \hat{\mathbf{x}}^o = \frac{\mathbf{v}^i}{\|\mathbf{v}^i\|_2},\ \hat{\mathbf{y}}^o = \frac{\hat{\mathbf{z}}^o \times \hat{\mathbf{x}}^o}{\|\hat{\mathbf{z}}^o \times \hat{\mathbf{x}}^o\|_2}, \quad (1)$$

where $\mathbf{r}^i$ and $\mathbf{v}^i$ are the distance between the spacecraft and the center of the Earth, and the inertial velocity of the spacecraft, respectively, in the ECI frame.

4) Wheel frame: Vectors in the wheel frame, denoted with a superscript $\{w\}$, have one element for each reaction wheel. The torque from each of the reaction wheels is given in the vector $\boldsymbol{\tau}_u^w \in \mathbb{R}^n$, where n is the number of reaction wheels. For this reason the wheel frame may not be a right handed coordinate frame for most reaction wheel configurations. The matrix $\mathbf{A} \in \mathbb{R}^{3\times n}$ maps the wheel frame to the body frame as follows [12]

$$\boldsymbol{\tau}_u^b = \mathbf{A}\boldsymbol{\tau}_u^w \implies \boldsymbol{\tau}_u^w = \mathbf{A}^+\boldsymbol{\tau}_u^b, \quad (2)$$

where the matrix $\mathbf{A}^+$ is the Moore-Penrose pseudo-inverse of $\mathbf{A}$ and $\boldsymbol{\tau}_u^b$ are the torques from the reaction wheels represented in the body frame. Due to a fixed reaction wheel configuration, $\mathbf{A}$ represents a constant mapping between $\{w\}$ and $\{b\}$.

B. Attitude representation

Unit quaternions are used to describe the attitude of the spacecraft. The unit quaternion, $\mathbf{q}_b^o$, denotes the attitude of $\{b\}$ relative to $\{o\}$. The rotation matrix from $\{o\}$ to $\{b\}$, $\mathbf{R}_o^b$ is defined as

$$\begin{aligned}\mathbf{R}_b^o &= \mathbf{R}(\mathbf{q}_b^o) = \mathbf{I}_{3\times3} + 2\eta_b^o\mathbf{S}(\boldsymbol{\epsilon}_b^o) + 2\mathbf{S}^2(\boldsymbol{\epsilon}_b^o),\\ \mathbf{R}_o^b &= (\mathbf{R}_b^o)^\top,\end{aligned} \quad (3)$$

where $\mathbf{q}_b^o = [\eta_b^o, \boldsymbol{\epsilon}_b^{o\top}]^\top \in \mathbb{R}^4$ satisfy the constraint $\eta^2 + \boldsymbol{\epsilon}_b^{o\top}\boldsymbol{\epsilon}_b^o = 1$, $\mathbf{I}_{3\times3}$ is the 3×3-identity matrix, and $\mathbf{S}(\cdot)$ is a skew-symmetric matrix. The time derivative of $\mathbf{R}_o^b$ is given as $\dot{\mathbf{R}}_o^b = -\mathbf{S}(\boldsymbol{\omega}_{ob}^b)\mathbf{R}_o^b$, where the angular velocities of $\{b\}$ relative to $\{o\}$ are given by $\boldsymbol{\omega}_{ob}^b$.

The kinematic differential equation for the spacecraft's attitude $\mathbf{q}_b^o$, is given by [11]

$$\dot{\mathbf{q}}_b^o = \begin{bmatrix}\dot{\eta}_b^o\\ \dot{\boldsymbol{\epsilon}}_b^o\end{bmatrix} = \frac{1}{2}\begin{bmatrix}-\boldsymbol{\epsilon}_b^{o\top}\\ \eta_b^o\mathbf{I}_{3\times3} + \mathbf{S}(\boldsymbol{\epsilon}_b^o)\end{bmatrix}\boldsymbol{\omega}_{ob}^b = \frac{1}{2}\mathbf{T}(\mathbf{q}_b^o)\boldsymbol{\omega}_{ob}^b, \quad (4)$$

where $\mathbf{T}(\cdot)$ denotes the angular velocity transformation matrix.

C. Angular velocity

When analysing the attitude of a spacecraft orbiting the Earth, three different angular velocities are of interest, namely the angular velocities of $\{b\}$ relative to $\{o\}$, $\boldsymbol{\omega}_{ob}^b$, the angular velocities of $\{o\}$ relative to $\{i\}$, $\boldsymbol{\omega}_{io}^b$, and the angular velocities of $\{b\}$ relative to $\{i\}$, $\boldsymbol{\omega}_{ib}^b$. The angular velocities relate to one another as follows:

$$\boldsymbol{\omega}_{ob}^b = \boldsymbol{\omega}_{ib}^b - \boldsymbol{\omega}_{io}^b = \boldsymbol{\omega}_{ib}^b - \mathbf{R}_o^b\boldsymbol{\omega}_{io}^o, \quad (5)$$

where $\boldsymbol{\omega}_{io}^o$ is defined as [13]

$$\boldsymbol{\omega}_{io}^o = \mathbf{R}_i^o\frac{\mathbf{S}(\mathbf{r}^i)\mathbf{v}^i}{(\mathbf{r}^i)^\top\mathbf{r}^i}. \quad (6)$$

Moreover, the inertial acceleration of the spacecraft is defined as

$$\dot{\mathbf{v}}^i = -\frac{GM}{\|\mathbf{r}^i\|_2^3}\mathbf{r}^i, \quad (7)$$

where G is the gravitational constant, M is the total mass of the Earth, and $\|\mathbf{r}^i\|_2$ denotes the 2-norm of $\mathbf{r}^i$. The rate of change for $\mathbf{r}^i$ is given as

$$\dot{\mathbf{r}}^i = \mathbf{v}^i. \quad (8)$$

D. Total system dynamics

The total spacecraft dynamics for a spacecraft orbiting the Earth are given as [2], [12]–[14]

$$\dot{\mathbf{q}}_b^o = \frac{1}{2}\mathbf{T}(\mathbf{q}_b^o)\boldsymbol{\omega}_{ob}^b \quad (9a)$$

$$\dot{\boldsymbol{\omega}}_{ib}^b = \mathbf{J}_s{}^{-1}(-\mathbf{A}\boldsymbol{\tau}_u^w - \mathbf{S}(\boldsymbol{\omega}_{ib}^b)\mathbf{J}\boldsymbol{\omega}_{ib}^b + \mathbf{A}\mathbf{J}_w\boldsymbol{\omega}_{bw}^w) \quad (9b)$$

$$\dot{\boldsymbol{\omega}}_{ob}^b = \dot{\boldsymbol{\omega}}_{ib}^b + \mathbf{S}(\boldsymbol{\omega}_{ob}^b)\mathbf{R}_o^b\boldsymbol{\omega}_{io}^o + \mathbf{R}_o^b\mathbf{S}(\mathbf{R}_b^o\boldsymbol{\omega}_{ob}^b)\boldsymbol{\omega}_{io}^o \quad (9c)$$

$$\dot{\boldsymbol{\omega}}_{bw}^w = \mathbf{J}_w{}^{-1}\boldsymbol{\tau}_u^w - \mathbf{A}^\top\dot{\boldsymbol{\omega}}_{ib}^b, \quad (9d)$$

where $\mathbf{J} \in \mathbb{R}^{3\times3}$ is the total system inertia of the spacecraft rigid body, defined as $\mathbf{J} = \mathbf{J}_s + \mathbf{A}\mathbf{J}_w\mathbf{A}^\top$, where $\mathbf{J}_s \in \mathbb{R}^{3\times3}$ denotes the inertia of the spacecraft rigid body excluding the inertia about the spinning axes of the reaction wheels, and $\mathbf{J}_w \in \mathbb{R}^{n\times n}$ denotes the inertia matrix of the reaction wheels about the spinning axes. Note that $\dot{\boldsymbol{\omega}}_{ib}^b = \frac{{}^bd}{dt}\boldsymbol{\omega}_{ib}^b$, $\dot{\boldsymbol{\omega}}_{ob}^b = \frac{{}^bd}{dt}\boldsymbol{\omega}_{ob}^b$, and $\dot{\boldsymbol{\omega}}_{bw}^w = \frac{{}^bd}{dt}\boldsymbol{\omega}_{bw}^w$.

III. MAXIMUM HANDS-OFF CONTROL

A. Mathematical preliminaries

The content presented in this section is based on [9], which provides a detailed review of the mathematics behind maximum hands-off control.

The L_1-norm of a vector $\mathbf{x} \in \mathbb{R}^{n_x}$ is defined as

$$\|\mathbf{x}\|_1 \triangleq \sum_{i=1}^{n_x}|x_i|. \quad (10)$$

The L_p-norm, with $p \in [1,\infty)$, of a vector of continuous-time signals $\mathbf{u}(t)$ over the time interval $[0,T)$ is defined as

$$\|\mathbf{u}\|_p \triangleq \left(\int_0^T \|\mathbf{u}(t)\|^p dt\right)^{\frac{1}{p}}. \quad (11)$$

The norm $\|\cdot\|$ inside the integral in (11) can be any p-norm for $p \in [1,\infty)$ [15]. If $p \in (0,1)$, in (11), then $\|\cdot\|_p$ is not a norm as it fails to satisfy the triangle inequality [9].

The support of a function is the set of points where the function takes on nonzero values [16], and the support set of a function $u(t)$, supp$(u(t))$, is defined by the closure of the set [9]

$$\{t \in [0,T] : u(t) \neq 0\}, \quad (12)$$

and by using (12), the L_0-norm of a continuous-time signal $u(t)$ can be defined by the length of the support of $u(t)$ accordingly:

$$\|u\|_0 \triangleq \mu(\text{supp}(u(t))), \tag{13}$$

where $\mu(\cdot)$ is the Lebesgue measure on $\mathbb{R}$.

B. Maximum Hands-off Control Problem Formulation

The maximum hands-off control is the control that maximizes the time interval over which the control input is exactly zero. To put it more precisely, the controller minimizes the Lebesgue measure of the support, i.e., the L_0-norm, to find the sparsest of the admissible controls [9]. The L_0-cost function is given as [9]

$$J_0(\mathbf{u}) \triangleq \sum_{i=1}^{m} \lambda_i \|u_i\|_0, \tag{14}$$

where m is the number of control inputs, $\mathbf{u}$ is the control input vector, λ_i are positive weights, and u_i denotes each element i in $\mathbf{u}$. The control that minimizes (14) is called the *maximum hands-off control*, or the L_0*-optimal control*, and it is the sparsest control among all admissible controls [9].

The L_0-cost function in (14) is discontinuous and non-convex [9]. Solving discontinuous and non-convex optimization problems are generally hard [9], and solving the L_0-optimal control problem is NP-hard [17]. Several relaxation methods and reformulations have been suggested to (14), for instance replacing the L_0-norm by the L_1-norm [9].

By defining the L_0-optimal control problem as [17]

$$\begin{aligned} \underset{\mathbf{x}}{\text{minimize}} \quad & f(\mathbf{x}) + \gamma\|\mathbf{x}\|_0 && \text{(15a)}\\ \text{subject to} \quad & c_i(\mathbf{x}) = 0,\ i \in \mathcal{E} && \text{(15b)}\\ & c_i(\mathbf{x}) \leq 0,\ i \in \mathcal{I}, && \text{(15c)} \end{aligned}$$

the L_0-optimal control problem can be reformulated using a set of complementarity constraints [17] accordingly,

$$\begin{aligned} \underset{\mathbf{x}}{\text{minimize}} \quad & f(\mathbf{x}) + \boldsymbol{\gamma}^\top(\mathbf{1}_N - \boldsymbol{\xi}) && \text{(16a)}\\ \text{subject to} \quad & c_i(\mathbf{x}) = 0,\ i \in \mathcal{E} && \text{(16b)}\\ & c_i(\mathbf{x}) \leq 0,\ i \in \mathcal{I} && \text{(16c)}\\ & \boldsymbol{\xi} \leq \mathbf{1}_N && \text{(16d)}\\ & \pm\boldsymbol{\xi} \circ \mathbf{x} \leq \epsilon\mathbf{1}_N && \text{(16e)}\\ & \boldsymbol{\xi} \geq \mathbf{0}, && \text{(16f)} \end{aligned}$$

where $\mathbf{1}_N$ is the N-vector of ones, N is the number of control intervals, and $\mathbf{1}_N - \boldsymbol{\xi}$ is the support vector of $\mathbf{x}$. The support $1-\xi_j$ of the state x_j essentially plays the same role as the support, supp$(\cdot)$, in (12). The notation $\mathbf{a} \circ \mathbf{b}$ denotes the componentwise product between the vectors $\mathbf{a}$ and $\mathbf{b}$. $\mathcal{E}$ and $\mathcal{I}$ are two finite index sets, $\boldsymbol{\gamma} > 0$ is a positive vector with components $\gamma_j > 0$, $f(\cdot)$ is the continuously differentiable objective function, and c_i the continuously differentiable constraint functions. $\epsilon > 0$ is a relaxation scalar. It is desirable to investigate the properties of the relaxed problem when ϵ approaches zero, because then the complementarity constraints would equal zero.

IV. CONTROL DESIGN

A. Control objectives

The control objective of the maximum hands-off controller is to find the sparsest control among all admissible control sequences. Note that for the remaining parts of this study, the term *sparsity* is defined in the following way:

Definition 4.1 (Sparsity): The *sparsity* of a control signal refers to the total time for which the control signal takes on nonzero values.

Minimizing the number of time intervals in which the control signal takes on nonzero values, a related concept, is referred to as minimum switching control. Minimum switching control has been studied for attitude control in [18].

Although the maximum hands-off controller yields the sparsest control, the control might not occur at the most favorable instants of time, which motivates the design of the moving maximum hands-off controller. The term *moving* refers to the characteristic of the controller which lets the user move the sparse control according to a desired set of preferences, for instance environmental conditions. In some situations, it may be ideal to not have any control input on a satellite, e.g., when a scientific measurement takes place. Using the moving maximum hands-off controller could facilitate that no control is applied during the time interval at which the measurement occurs.

B. Maximum hands-off controller

The maximum hands-off controller, or the L_0-optimal controller, aims to minimize the L_0-norm of the control input. The design of the maximum hands-off controller implemented in this paper is inspired by the relaxed formulation in (16) with $\boldsymbol{\gamma} = \mathbf{1}_N$, and is formulated as

$$\begin{aligned} \underset{\boldsymbol{\tau}_u^b, \boldsymbol{\xi}}{\text{minimize}} \quad & k_1 f(\boldsymbol{\omega}_{ob}^b) + k_2 g(\mathbf{q}_b^o) + k_3(\mathbf{1}_N - \boldsymbol{\xi})\mathbf{1}_N^\top && \text{(17a)}\\ \text{subject to} \quad & \dot{\mathbf{x}} = \mathbf{f}(\mathbf{x}, \boldsymbol{\tau}_u^b) && \text{(17b)}\\ & \pm\boldsymbol{\tau}_u^w \leq \boldsymbol{\tau}_{\text{limit}} && \text{(17c)}\\ & \mathbf{x}(0) = \mathbf{x}_0 && \text{(17d)}\\ & \boldsymbol{\xi} \leq \mathbf{1}_N && \text{(17e)}\\ & \pm\boldsymbol{\xi} \circ \boldsymbol{\tau}_{u,1}^b \leq \epsilon\mathbf{1}_N && \text{(17f)}\\ & \pm\boldsymbol{\xi} \circ \boldsymbol{\tau}_{u,2}^b \leq \epsilon\mathbf{1}_N && \text{(17g)}\\ & \pm\boldsymbol{\xi} \circ \boldsymbol{\tau}_{u,3}^b \leq \epsilon\mathbf{1}_N && \text{(17h)}\\ & \boldsymbol{\xi} \geq \mathbf{0}, && \text{(17i)} \end{aligned}$$

where k_1, k_2 and k_3 are positive constants, $\boldsymbol{\xi}$ is the complementarity vector to the control input $\boldsymbol{\tau}_u^b$, and $\mathbf{1}_N - \boldsymbol{\xi}$ is the support vector of $\boldsymbol{\tau}_u^b$. $\boldsymbol{\tau}_{u,1}^b$, $\boldsymbol{\tau}_{u,2}^b$, and $\boldsymbol{\tau}_{u,3}^b$ denotes the components of $\boldsymbol{\tau}_u^b$ about the x, y and z-axis in $\{b\}$, respectively. The state vector $\mathbf{x}$ is defined by $[\mathbf{q}_b^{o\top}, \boldsymbol{\omega}_{ib}^{b\top}, \boldsymbol{\omega}_{ob}^{b\top}, \boldsymbol{\omega}_{bw}^{w\top}, \mathbf{v}^{i\top}, \mathbf{r}^{i\top}]^\top$, $\mathbf{x}_0$ denotes the initial state values, and $\mathbf{f}(\mathbf{x}, \boldsymbol{\tau}_u^b)$ is defined by (9a), (9b), (9c), (9d), (7), and (8). The functions $f(\cdot)$ and $g(\cdot)$ are

designed to steer $\boldsymbol{\omega}_{ob}^{b}$ and $\mathbf{q}_{b}^{o}$, respectively, to their desired final states. More specifically,

$$\begin{aligned} f(\boldsymbol{\omega}_{ob}^{b}) &= \sum_{i=1}^{n_\omega} (\omega_{ob,i}^{b}(T) - \omega_{ob,\text{ref},i}^{b})^2 \\ g(\mathbf{q}_{b}^{o}) &= 1 - \left| (\mathbf{q}_{b}^{o}(T))^\top \mathbf{q}_{b,\text{ref}}^{o} \right|, \end{aligned} \tag{18}$$

where T denotes the final time, $\boldsymbol{\omega}_{ob,\text{ref}}^{b}$ and $\mathbf{q}_{b,\text{ref}}^{o}$ are the reference angular velocities and reference quaternion, n_ω denotes the number of entries in $\boldsymbol{\omega}_{ob}^{b}(T)$ and $\boldsymbol{\omega}_{ob,\text{ref}}^{b}$, and $\omega_{ob,i}^{b}(T)$ and $\omega_{ob,\text{ref},i}^{b}$ denotes the ith component of $\boldsymbol{\omega}_{ob}^{b}(T)$ and $\boldsymbol{\omega}_{ob,\text{ref}}^{b}$, respectively. The function $g(\cdot)$ is a pseudometric on the unit quaternion, but a metric on $SO(3)$ [19]. The absolute value, $|(\mathbf{q}_{b}^{o}(T))^\top \mathbf{q}_{b,\text{ref}}^{o}|$, is approximated as $\max\left((\mathbf{q}_{b}^{o}(T))^\top \mathbf{q}_{b,\text{ref}}^{o}, -(\mathbf{q}_{b}^{o}(T))^\top \mathbf{q}_{b,\text{ref}}^{o}\right)$ [20].

C. Moving maximum hands-off controller

The design of the moving maximum hands-off controller is similar to that of the maximum hands-off controller in (17). The moving maximum hands-off optimal control problem is formulated as

$$\underset{\boldsymbol{\tau}_u^b, \boldsymbol{\xi}}{\text{minimize}} \quad k_1 f(\boldsymbol{\omega}_{ob}^{b}) + k_2 g(\mathbf{q}_{b}^{o}) + k_3 (\mathbf{1}_N - \boldsymbol{\xi} \circ \mathbf{h}_N) \mathbf{1}_N^\top, \tag{19}$$

where the constraints on (19) are identical to (17b) to (17i). The vector $\mathbf{h}_N$ specifies where the control torques should occur. By default, the vector $\mathbf{h}_N$ is an N-dimensional vector of all ones. The user might change the values of $\mathbf{h}_N$ to values between 0 and 1, to indicate for which time intervals the control input should occur. For instance, if the value of $\mathbf{h}_N$ is set to 0.1 for $N = 10, \ldots, 20$, it would yield a more optimal solution if the control occur between these control intervals as sparsity comes at a lower cost in this interval than the rest.

D. L_1-optimal controller

The design of the L_1-optimal control problem is formulated as

$$\underset{s, \boldsymbol{\tau}_u^b}{\text{minimize}} \quad k_1 f(\boldsymbol{\omega}_{ob}^{b}) + k_2 g(\mathbf{q}_{b}^{o}) + k_3 \sum_{i=0}^{N} s_k \tag{20}$$

where (20) is constrained by (17b) to (17d), in addition to $-\mathbf{s}_N \leq \boldsymbol{\tau}_u^b \leq \mathbf{s}_N$. $\sum_{i=0}^{N} s_k$ denotes the L_1-norm of $\boldsymbol{\tau}_u^b$, i.e., $\|\boldsymbol{\tau}_u^b\|_1 = \sum_{i=0}^{n} s_i = \mathbf{1}^\top \mathbf{s}$, where $\mathbf{s} \in \mathbb{R}^n$ is a set of slack variables [21].

E. PD-controller

A standard PD controller is given as [1]

$$\boldsymbol{\tau}_u^b = \mathbf{K}_d \boldsymbol{\omega}_e^b + \mathbf{K}_p \boldsymbol{\epsilon}_e. \tag{21}$$

Here, $\boldsymbol{\omega}_e^b$ is the angular velocity error, defined as $\boldsymbol{\omega}_e^b = \boldsymbol{\omega}_{ob}^{b} - \boldsymbol{\omega}_d^b$, where $\boldsymbol{\omega}_d^b$ is the desired angular velocity. $\boldsymbol{\epsilon}_e$ is the vector part of the error quaternion, defined as $\mathbf{q}_e = \mathbf{q}_d^{-1} \otimes \mathbf{q}_b^o$, where $\mathbf{q}_d = [\eta_d, \boldsymbol{\epsilon}_b^\top]^\top$ is the desired attitude. $\mathbf{K}_d$ and $\mathbf{K}_p$ are constant and positive definite controller gain matrices. The numerical values of the gain matrices were chosen while tuning the PD controller.

V. SIMULATION SETUP

The experiments were conducted using CasADi as the optimization tool [22]. The NLP-solver IPOPT was used to solve the optimization problems, using the solver's default options. The optimal control problems in (17), (19) and (20) were discretized using direct multiple-shooting, whereas the dynamics of the spacecraft were discretized using Runge-Kutta 4 integration. The output from the PD controller was used as the initial guesses for the L_1-optimal controller, and the output from the L_1-optimal controller was given as initial guesses for the maximum hands-off controller and the moving maximum hands-off controller. The initial guesses were applied to the states $\boldsymbol{q}_b^o$, $\boldsymbol{\omega}_{ib}^b$, and $\boldsymbol{\omega}_{bw}^w$. No initial guesses were applied to the control torque $\boldsymbol{\tau}_u^b$, i.e., the default initial guess of zero used by CasADi was applied.

Some tests were conducted with different initial guesses to see how the controllers responded. The tests revealed that the initial guesses for IPOPT are of significant importance when trying to find the optimal solutions. Different initial guesses causes the optimization to iterate fast or slow towards an optimal solution, and affect the quality of the solution [23].

The experiments reported in this paper were conducted using a 2 GHz Intel Core i7-9700T CPU computer running Windows. The simulation of the experiments were conducted using the parameters for a 6U CubeSat as the spacecraft rigid body, and it is assumed to orbit in Low-Earth-Orbit (LEO). Four reaction wheels are used to control the attitude of the CubeSat. This is part of the setup that is going to be used for the HYPSO-1 mission, which motivates the work in this paper [10]. Three of the reaction wheels are placed orthogonally along the three axes of the body frame. The fourth reaction wheel is placed such that it's torque yields equal components in each of the body axes. The torque distribution matrix $\mathbf{A}$ is given as [12]

$$\mathbf{A} = \begin{bmatrix} 1 & 0 & 0 & \frac{1}{\sqrt{3}} \\ 0 & 1 & 0 & \frac{1}{\sqrt{3}} \\ 0 & 0 & 1 & \frac{1}{\sqrt{3}} \end{bmatrix}. \tag{22}$$

The total inertia matrix for the spacecraft rigid body and the inertia matrix of the reaction wheels are given as [12]

$$\mathbf{J} = \begin{bmatrix} 0.0775 & 0.0002 & -0.0002 \\ 0.0002 & 0.1067 & 0.0005 \\ -0.0002 & 0.0005 & 0.0389 \end{bmatrix} \text{kg}\cdot\text{m}^2, \; \mathbf{J}_w = J_w \mathbf{I}_{4\times 4}, \tag{23}$$

where $J_w = 2.1 \cdot 10^{-4}$ kg·m^2 is the inertia of a single reaction wheel. The controller gains, and the parameters required for the optimization are shown in Table I.

After the final optimization procedure finishes, the system is propagated for an additional number of control intervals, denoted N_{prop}, to visualize the post-optimization response of the system. The final state from the optimization serves as the initial state for the propagation, and the control input is set to zero for the whole propagation. The orbit of the spacecraft is initialized using the orbital parameters in Table I, which are transformed into ECI coordinates using the RANDV-function

TABLE I

CONTROLLER GAINS, OPTIMIZATION CONSTANTS, AND ORBITAL PARAMETERS.

Parameter	Value	Unit
k_1	$1 \cdot 10^6$	s^2
k_2	$1 \cdot 10^2$	-
k_3	$1 \cdot 10^1$	-
$\mathbf{K}_p$	$3 \cdot \mathbf{J}_s$	N·m
$\mathbf{K}_d$	$2.7 \cdot \mathbf{J}_s$	N·m·s
Simulation time (T)	70	s
Control intervals (N)	50	-
Step size (h)	1.4	s
Control intervals for propagation (N_{prop})	20	-
ϵ	$1 \cdot 10^{-8}$	-
τ_{limit}	$\pm 3 \cdot 10^{-3}$	N·m
Semi-major axis	6852.2	km
Eccentricity	0.002	-
Inclination	97	$^\circ$
Right ascension of the ascending node	280	$^\circ$
Argument of periapsis	0	$^\circ$
True anomaly	0	$^\circ$
Standard grav. parameter, Earth (GM)	$3.986 \cdot 10^{14}$	m^3/s^2

from [24]. Two types of simulations were conducted: a single-axis maneuver where the satellite rotates 45° about the x-axis, and a multiple-axis maneuver where satellite rotates about all three axes of the chosen frames.

VI. RESULTS

Fig. 1 shows the change in the spacecraft's attitude over time using the Euler angle representation, and reveals that all three controllers are able to steer the spacecraft to the desired orientation of $(\phi, \theta, \psi) = (45^\circ, 0^\circ, 0^\circ)$ and keep the spacecraft at this attitude. The dotted lines ϕ_d, θ_d, and ψ_d denotes the angles of the desired attitude, whereas the solid lines ϕ, θ, and ψ corresponds to the actual states. The orange area in the moving L_0-section of the figures shows the placement of the interval where $\mathbf{h}_N$ takes lower values. For the rest of the interval, $\mathbf{h}_N$ is set to 1. The torque vector $\boldsymbol{\tau}_u^b$ can be seen in Fig. 2. The torque vector $\boldsymbol{\tau}_u^w$ can be seen in Fig. 3. The angular velocities $\boldsymbol{\omega}_{ob}^b$ are shown in Fig. 4 and reveal that the spacecraft stops rotating, i.e., $\{b\}$ stops rotating relative to $\{o\}$, when the desired orientation is reached. The angular velocities $\boldsymbol{\omega}_{bw}^w$ can be seen in Fig. 5, and illustrate the dynamical response of the reaction wheels. The computation times, the sparsity, and the number of iterations used to find the optimal solution for each of the three controllers are shown in Table II.

TABLE II

COMPUTATION TIME, SPARSITY AND NUMBER OF ITERATIONS SINGLE-AXIS MANEUVER.

Controller	CPU time NLP, [s]	CPU time IPOPT, [s]	Sparsity, [s]	Iterations
L_0	3.235	0.253	2.8	25
Moving L_0	46.914	3.828	2.8	371
L_1	2.479	0.204	2.8	19

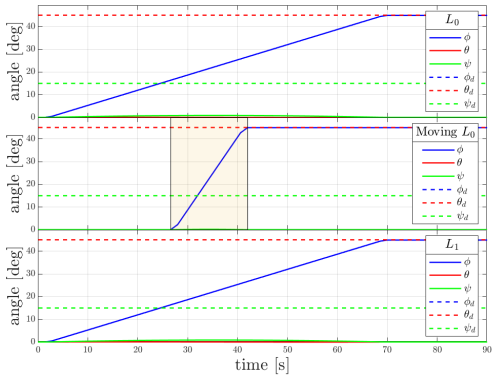

Fig. 1. Euler angles, single-axis maneuver.

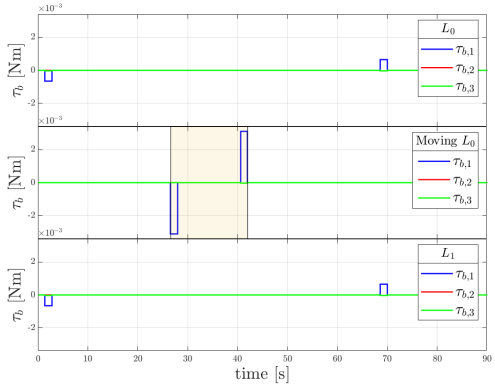

Fig. 2. Control input in $\{b\}$, single-axis maneuver.

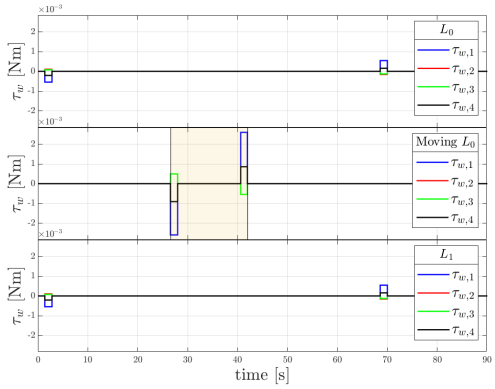

Fig. 3. Control input in $\{w\}$, single-axis maneuver.

Fig. 6 shows the change in the spacecraft's attitude over time from a multiple-axis maneuver from $(\phi, \theta, \psi) = (0^\circ, 0^\circ, 0^\circ)$ to $(90^\circ, 45^\circ, 15^\circ)$. The optimal control torques $\boldsymbol{\tau}_u^b$ and $\boldsymbol{\tau}_u^w$ are shown in Fig. 7 and Fig. 8, respectively. The angular velocities $\boldsymbol{\omega}_{ob}^b$ are shown in Fig. 9. The angular velocities $\boldsymbol{\omega}_{bw}^w$ are shown in Fig. 10. The computation times, the sparsity, and the number of iterations used to find the optimal solution for each of the three controllers are shown in Table III.

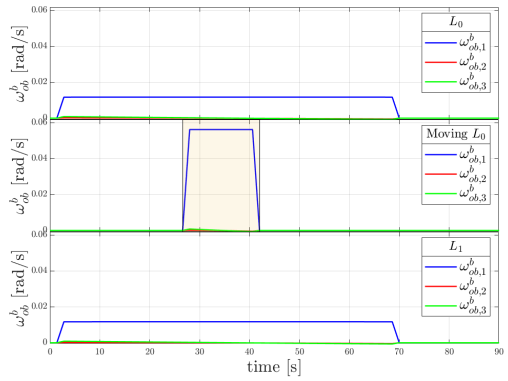

Fig. 4. Angular velocities, $\boldsymbol{\omega}^b_{ob}$, single-axis maneuver.

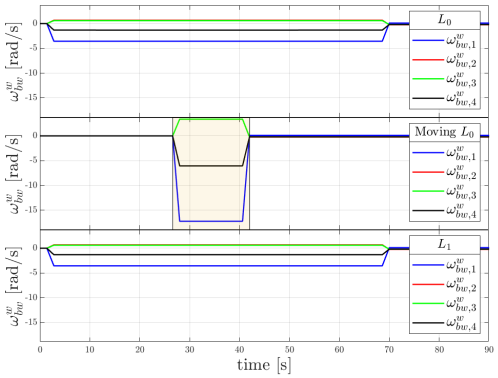

Fig. 5. Angular velocities, $\boldsymbol{\omega}^w_{bw}$, single-axis maneuver.

TABLE III

COMPUTATION TIME, SPARSITY AND NUMBER OF ITERATIONS MULTIPLE-AXIS MANEUVER.

Controller	**CPU time NLP, [s]**	**CPU time IPOPT, [s]**	**Sparsity, [s]**	**Iterations**
L_0	66.216	6.106	2.8	497
Moving L_0	90.175	7.706	2.8	699
L_1	5.131	0.360	2.8	39

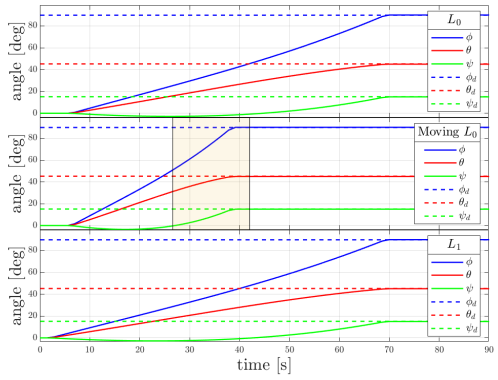

Fig. 6. Euler angles, multiple-axis maneuver.

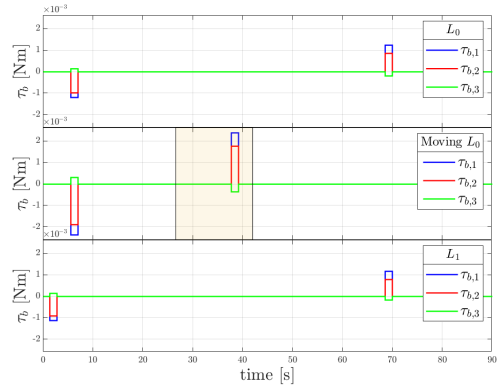

Fig. 7. Control input in $\{b\}$, multiple-axis maneuver.

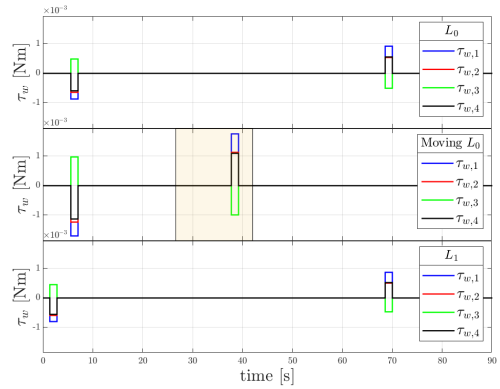

Fig. 8. Control input in $\{w\}$, multiple-axis maneuver.

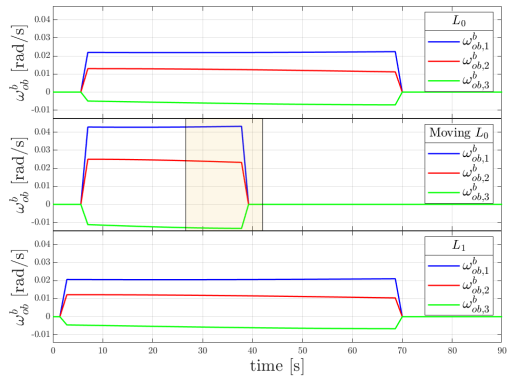

Fig. 9. Angular velocities, $\boldsymbol{\omega}^b_{ob}$, multiple-axis maneuver.

VII. DISCUSSION

In this section, the maximum hands-off controller will be referred to as the L_0-optimal controller or the L_0-controller, whereas the moving maximum hands-off controller will be referred to as the moving L_0-optimal controller or the moving L_0-controller. The *sparsity* of a control signal is defined in Definition 4.1.

A. Single-axis

Figs. 1 to 4 show that the spacecraft's state space trajectories and the control signals are identical for the L_0-controller

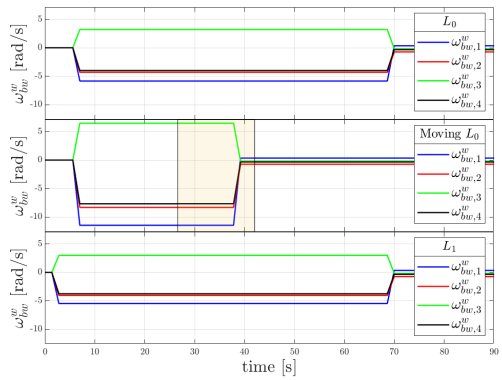

Fig. 10. Angular velocities, $\boldsymbol{\omega}_{bw}^{w}$, multiple-axis maneuver.

and the L_1-controller. These results are in agreement with the findings in [9], and suggests that the L_1-norm may be used as an approximation to the L_0-norm.

As Figs. 1 to 4 show, the spacecraft's state space trajectories and the control signals resulting from the moving L_0-controller differ from the two other controllers. The differences can be explained by comparing the cost functions of the three controllers in (17a), (19), and (20). For the moving L_0-controller, the vector $\mathbf{h}_N$ was chosen such that it would cost less for the control inputs to occur between $t = 28$ s and $t = 42$ s. For the two other controllers, it is equally expensive for the control inputs to occur over the whole time interval. Fig. 2 and Fig. 3 show that the control inputs produced by the moving L_0-controller occur at $t = 28$ s and $t = 42$ s, and Fig. 1 and Fig. 4 show that the spacecraft's states change within this interval.

As can be seen in Fig. 2 and Fig. 3, the optimal control signal computed by the moving L_0-controller has larger amplitude than the control signals produced by the two other controllers. A possible explanation for this is that since the moving L_0-control torques occur closer in time, the torque applied at each of the two time instants has to be larger in order to steer the spacecraft to the desired orientation within a smaller time interval. If the time interval was larger, the control inputs could be smaller as the spacecraft would have more time to rotate towards the desired orientation after the initial control input has been applied.

Fig. 2 and Fig. 3 show that the control inputs produced by the moving L_0-controller occur at $t = 28$ s and $t = 42$ s, which means that they occur exactly at the boundaries of the time interval specified by $\mathbf{h}_N$. The saturation limits for the control torque are $\tau_{\text{limit}} = \pm 3 \cdot 10^{-3}$ N·m, and Fig. 3 shows that the control torques produced by the moving L_0-controller are close to the saturation limits. If the control torques had occurred at other time instants in the interval specified by $\mathbf{h}_N$, they would occur closer in time and the torques would therefore have larger values. The control torques are already close to the saturation limits when they occur at $t = 28$ s and $t = 42$ s, and if the torque values were to increase the reaction wheels may saturate. If the reaction wheels saturate, an additional control torque may be required to perform the spacecraft maneuver, and an additional control torque would yield a less sparse control signal. It is cheaper for the control input to occur between $t = 28$ s and $t = 42$ s, but if the control torques are too close in time they may saturate. Then, the controller would have to apply an additional control torque which would result in a less sparse control signal. Therefore, it makes sense that the control torques occur at the borders of the time interval specified by $\mathbf{h}_N$, i.e., at $t = 28$ s and $t = 42$ s.

Table II shows that all three controllers yield optimal control signals which have the same sparsity. This finding confirms that all three controllers are able find the sparsest solution. For this type of spacecraft single-axis maneuver, it is not possible to find a control signal sparser than 2 time steps, which means a total signal length of 2.8 s, as one control torque has to push the spacecraft towards the desired attitude and one control input has to stop the spacecraft rotation. For the conditions provided in this paper, a control signal in which torques occur at two different time instants provides the sparsest optimal control signal for the spacecraft single-axis maneuver.

When trying to maneuver the spacecraft an angle $\phi = 45°$ about the x-axis, one might expect an optimal controller to yield control torque simply about the body-frame x-axis. Fig. 2 shows that control torques are applied about all three axes, although the control torque about the x-axis is the most prominent. The reason why the optimal control algorithms yield torque about all three axes is because the spacecraft rotates relative to it's orbit at the same time as it orbits the Earth. A spacecraft in orbit, such as the one used in this work, would rotate relative to its orbit, which results in the angular velocity dynamics in (9c). Because of the spacecraft's rotation around the Earth, there will be rotation about the y- and z-axis throughout the optimization horizon, in addition to the control effort made about the x-axis. Therefore, torque from the reaction wheels has to be applied to compensate for the drift about the y- and z-axis.

The total inertia matrix for the spacecraft rigid body, $\mathbf{J}$, in (23) also contributes to rotation about multiple axes. Due to the nonlinearity of the spacecraft dynamics, the terms are coupled, which results in torque about all three axes, even though motion is only needed about one axis. The total system inertia matrix given in (23) is not diagonal. If a diagonal $\mathbf{J}$-matrix were used instead of the one in (23), the states would be less coupled, which is clear from (9b). Less coupling of the dynamics would yield less torque about the y- and z-axis, when a maneuver is performed about the x-axis.

B. Multiple-axis maneuver

Fig. 7 and Fig. 8 show that the first control torque from the moving L_0-controller occurs after about $t = 5$ s, and the second control torque occurs close to $t = 40$ s. The second control torque occurs within the interval specified by $\mathbf{h}_N$. The vector $\mathbf{h}_N$ was chosen such that it would cost less for the control inputs to occur between $t = 28$ s and $t = 42$ s. One might have expected all control inputs to occur

within this time interval. However, one control input occurs outside this interval. The reason for this is that there are no constraints on where the control input should not occur; it only costs less between $t = 28$ s and $t = 42$ s. The optimization procedure aims to satisfy the constraints and to minimize the cost function, which is also a function of the final state values. If it is not possible to reach this goal by applying control input within the cheap interval specified by $\mathbf{h}_N$, some or all of the control input will occur outside this interval. Therefore, control inputs may occur outside the interval defined by $\mathbf{h}_N$. Should it be desirable to force control inputs at any point to zero, adding a constraint on the input would be a possible solution.

The L_1-optimal control signal and L_0-optimal control signal are not identical, which can be seen in Fig. 7 and Fig. 8. The first control input produced by the L_1-controller occurs before the first control input produced by the L_0-controller, whereas the two last control inputs occur simultaneously. The amplitude of the control torques from the L_1-controller are smaller than those from the L_0-controller. A possible explanation for the difference in amplitudes is that since there are more time between the two L_1-control inputs, the spacecraft will have more time to rotate to the desired orientation, and thus less torque would need to be applied. Therefore, it makes sense that the control torque produced by the L_1-controller are smaller than the control torque produced by the L_0-controller. These results suggest that the L_1-optimal solution does not always equal the L_0-optimal solution. On the other hand, they suggest that the L_1-optimal control problem could be an acceptable approximation to the L_0-optimal control problem.

VIII. CONCLUSION

The main goal of this paper has been to explore the use of maximum hands-off control, also called L_0-optimal control, for the spacecraft attitude control problem. Our work has shown that the maximum hands-off controller is able to steer the spacecraft to the desired attitude and the desired final states. Thus, our work confirms that the maximum hands-off controller works for the spacecraft attitude control problem. The use of the moving maximum hands-off controller has also been explored for the spacecraft attitude control problem. Our findings suggest that the controller works as intended, which means that the controller produces a control signal that can be moved to a predefined interval specified by the vector $\mathbf{h}_N$. While the cost in certain intervals might be lowered with the choice of $\mathbf{h}_N$, control torque may still occur outside this interval as the optimization procedure aims to satisfy the constraints while minimizing the cost function.

REFERENCES

[1] J.-Y. Wen and K. Kreutz-Delgado, "The attitude control problem," *IEEE Trans. Automat. Contr.*, vol. 36, no. 10, pp. 1148–1162, 1991.

[2] R. Kristiansen, P. J. Nicklasson, and J. T. Gravdahl, "Satellite attitude control by quaternion-based backstepping," *IEEE Trans. Control Syst. Technol.*, vol. 17, no. 1, pp. 227–232, 2008.

[3] G. Meyer, *Design and global analysis of spacecraft attitude control systems*. National Aeronautics and Space Administration, Ames Research Center, 1971.

[4] L.-L. Show, J.-C. Juang, C.-T. Lin, and Y.-W. Jan, "Spacecraft robust attitude tracking design: PID control approach," in *Proc. 2002 Am. Control Conf.*, vol. 2. IEEE, 2002, pp. 1360–1365.

[5] T. Lee, M. Leok, and N. H. McClamroch, "Time optimal attitude control for a rigid body," in *Proc. 2008 Am. Control Conf.* IEEE, 2008, pp. 5210–5215.

[6] J. D. Biggs and L. Colley, "Geometric attitude motion planning for spacecraft with pointing and actuator constraints," *J. Guid. Control Dyn.*, vol. 39, no. 7, pp. 1672–1677, 2016.

[7] T. Ikeda and M. Nagahara, "Time-optimal hands-off control for linear time-invariant systems," *Automatica*, vol. 99, pp. 54–58, 2019.

[8] D. Chatterjee, M. Nagahara, D. E. Quevedo, and K. M. Rao, "Characterization of maximum hands-off control," *Syst. Control. Lett.*, vol. 94, pp. 31–36, 2016.

[9] M. Nagahara, D. E. Quevedo, and D. Nešić, "Maximum hands-off control: a paradigm of control effort minimization," *IEEE Trans. Automat. Contr.*, vol. 61, no. 3, pp. 735–747, 2015.

[10] M. E. Grøtte, R. Birkeland, E. Honoré-Livermore, S. Bakken, J. L. Garrett, E. F. Prentice, F. Sigernes, M. Orlandić, J. T. Gravdahl, and T. A. Johansen, "Ocean Color Hyperspectral Remote Sensing With High Resolution and Low Latency—The HYPSO-1 CubeSat Mission," *IEEE Trans Geosci Remote Sens*, vol. 60, pp. 1–19, 2022.

[11] O. Egeland and J. T. Gravdahl, *Modeling and simulation for automatic control*, corr., 2. print ed. Trondheim: Marine Cybernetics AS, 2003.

[12] B. A. Kristiansen, M. E. Grøtte, and J. T. Gravdahl, "Quaternion-based generalized super-twisting algorithm for spacecraft attitude control," *IFAC-PapersOnLine*, vol. 53, no. 2, pp. 14 811–14 818, 2020, 21st IFAC World Congress.

[13] E. Oland and R. Schlanbusch, "Reaction wheel design for cubesats," in *Proc. 4th International Conference on Recent Advances in Space Technologies*. IEEE, 2009, pp. 778–783.

[14] T. R. Krogstad and J. T. Gravdahl, "6-DOF mutual synchronization of formation flying spacecraft," in *Proc. 45th IEEE Conf. Decis. Control*. IEEE, 2006, pp. 5706–5711.

[15] H. K. Khalil, *Nonlinear systems*. Prentice Hall, 2002.

[16] H. L. Royden and P. Fitzpatrick, *Real analysis*. Macmillan New York, 1988, vol. 32.

[17] M. Feng, J. E. Mitchell, J.-S. Pang, X. Shen, and A. Wächter, "Complementarity formulations of l0-norm optimization problems," *Industrial Engineering and Management Sciences. Technical Report. Northwestern University, Evanston, IL, USA*, 2016.

[18] A. Garulli, A. Giannitrapani, and M. Leomanni, "Minimum switching control for systems of coupled double integrators," *Automatica*, vol. 60, pp. 115–121, 2015.

[19] D. Q. Huynh, "Metrics for 3D rotations: Comparison and analysis," *J. Math. Imaging Vis.*, vol. 35, no. 2, pp. 155–164, 2009.

[20] B. A. Kristiansen, J. T. Gravdahl, and T. A. Johansen, "Energy optimal attitude control for a solar-powered spacecraft," *European Journal of Control*, vol. 62, pp. 192–197, 2021.

[21] S. Gros and M. Diehl, *Numerical Optimal Control (Draft)*, 2019.

[22] J. A. Andersson, J. Gillis, G. Horn, J. B. Rawlings, and M. Diehl, "CasADi: a software framework for nonlinear optimization and optimal control," *Math. Program. Comput.*, vol. 11, no. 1, pp. 1–36, 2019.

[23] S. K. Schaanning, "Maximum hands-off control for attitude control of a spacecraft," Master's thesis, Norwegian U. of Sci. and Tech, 2021.

[24] D. A. Vallado, *Fundamentals of astrodynamics and applications*. Springer Science & Business Media, 2001, vol. 12.